Zinc Porphyrin–Re(I) Bipyridyl–Fullerene Triad: Synthesis, Characterization, and Kinetics of the Stepwise Electron-Transfer Processes Initiated by Visible Excitation

Paolo Cavigli,[†] Tatiana Da Ros,[†] Axel Kahnt,[¶] Marta Gamberoni,[§] Maria Teresa Indelli,*[,§] and Elisabetta Iengo*[,†]

[†]Department of Chemical and Pharmaceutical Sciences, University of Trieste, Via L. Giorgieri 1, 34127 Trieste, Italy

[¶]Lehrstuhl für Physikalische Chemie I, Friedrich-Alexander-Universität Erlangen-Nürnberg, Egerlandstraße 3, 91058 Erlangen, Germany

[§]Department of Chemical and Pharmaceutical Sciences, University of Ferrara, Via Fossato di Mortara 17, 44121 Ferrara, Italy

Supporting Information

ABSTRACT: A new triad system featuring one zinc porphyrin and one fullerene moieties attached to a central redox-active Re(I) connector was obtained in remarkable yield by cleverly exploiting a facile two-step synthesis. Detailed description and discussion on the characterization of this multicomponent system and of its parent free-base analogue are presented, along with a kinetic study of the stepwise electron-transfer processes occurring upon visible excitation.

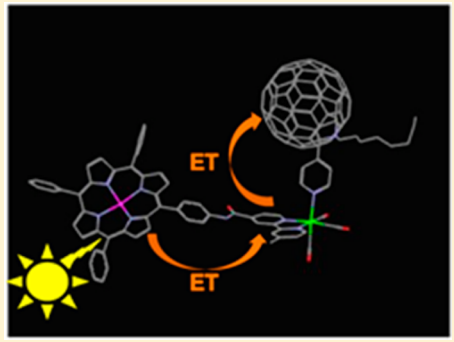

INTRODUCTION

Artificial photosynthesis, that is, the use of light energy to produce solar fuels, is a timely research field.[1] Photochemical water splitting, as an ideal energy-storing reaction, is the focus of worldwide research for applications in artificial photosynthesis; at the same time, large efforts are being devoted worldwide to the development of efficient molecular devices for photocatalytic reduction of CO_2.[2] The chemical conversion of CO_2 has been studied intensively by several groups with particular attention to the use of rhenium polypyridine photocatalysts.[3] The main drawback of these photocatalysts is the lack of absorption into the visible region. One of the major strategy to solve this problem is to build multicomponent conjugates containing one visible-light absorber unit connected to the rhenium catalyst. This approach has been investigated in recent years, in particular by the group of Ishitani[4a−c] and of Perutz.[4d,4e] From a structural point of view, the use of Re(I) is particularly effective in combination with N-based ligands, as strong and inert bonds are established. Indeed, this metal center has been employed in the construction of robust assemblies containing pyridyl porphyrins for multipurpose applications.[5]

In this context, we have previously reported on the synthesis and characterization of Re(I) zinc-porphyrin dyads, obtained employing, as common starting metal precursor, the complex [*fac*-$Re(CO)_3$(dmso-O)$_3$](OTf) (dmso = dimethyl sulfoxide; OTf = trifluoromethanesulfonate). This complex, as compared to the more commonly employed [$ReBr(CO)_5$], has been demonstrated to be very versatile as it allows the stepwise replacement of the three dmso-O with the desired ligands, under mild conditions.[6]

For the dyad reported in Chart 1, a detailed photophysical investigation has revealed the occurrence of a fast photoinduced electron transfer from the singlet excited state of the zinc-porphyrin chromophoric unit (ZnP) to the $Re(CO)_3$(bpy) fragment (Re) (bpy = 2,2′-bipyridine).[7] Ultrafast time-resolved techniques have shown that the charge-separated state [ZnP^+–$Re(CO)_3(bpy)^{\bullet-}$], formed upon visible excitation, recombines to the ground state in tens of picoseconds.[7]

The present work is aimed toward improving the performance of this dyad by introducing a third redox-active component, which should promote the formation of a charge-separated state over a longer distance. For this purpose, a three-component system containing a fullerene as second electron acceptor was designed (Chart 1). Among the possible electron acceptors, fullerene has been chosen for its peculiar properties: (i) low, and reversible, first reduction potential; (ii) small reorganization energy, which tends to increase the rate of charge separation and decrease that of charge recombination.[8]

While metalloporphyrin–fullerene conjugates have been investigated to a larger extent,[9] examples of fullerenes coordinated to metal complexes are quite rare.[10] To our

Chart 1

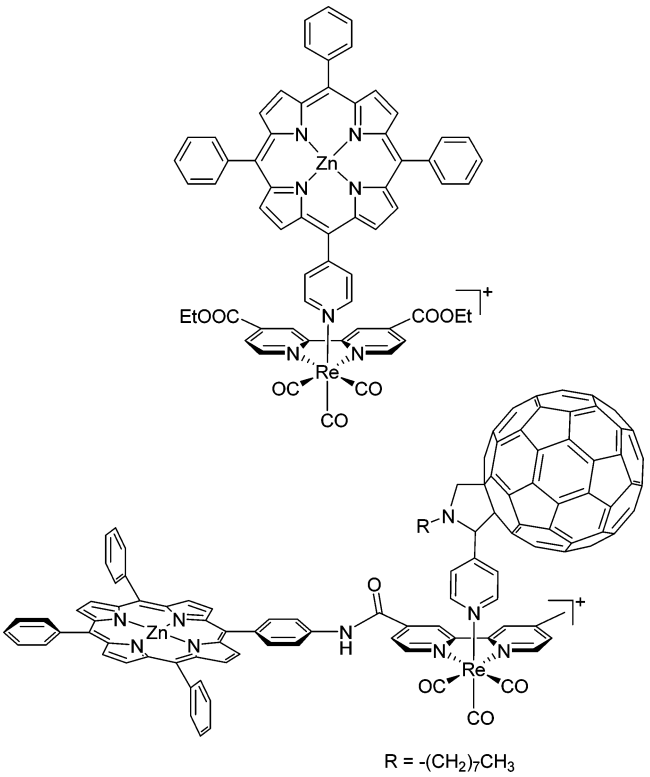

knowledge three-component systems containing a metalloporphyrin as chromophore and, as first and second electron acceptor, a metal complex and a fullerene, respectively, have never been described before.

In this work, the desired triad system (Chart 1) has been conveniently obtained by coordination, in a stepwise manner, to the [*fac*-$Re(CO)_3(dmso\text{-}O)_3]^+$ precursor of one zinc porphyrin and one fullerene, appropriately functionalized. In this system the rhenium fragment acts both as central coordinative connector and as redox-active unit. The synthesis, characterization, and photophystical properties of this new triad system will be discussed in detail here.

EXPERIMENTAL SECTION

Instrumental Methods. Mono- and bidimensional NMR experiments (^{1}H, H−H COSY, H−C COSY, H−H NOESY, ROESY) were recorded on a Varian 500 (500 MHz) spectrometer. All spectra were run at room temperature; ^{1}H chemical shifts were referenced to the peak of residual nondeuterated solvent (δ (ppm) = 7.26 ($CHCl_3$), 3.30 (CH_3OH), 2.50 (dmso), 4.33 (CH_3NO_2), and 8.03 (dimethylformamide (DMF)). Elemental analysis was performed at the Department of Chemical Sciences and Technologies, University of Udine (Italy). Electrospray ionization (ESI) mass spectrometry (MS) measurements were performed on a PerkinElmer APII spectrometer at 5600 eV by Dr. F. Hollan, Dept. of Chemical and Pharmaceutical Sciences, Univ. of Trieste, Italy. Solid IR spectra were recorded on a Varian 660-IR FT-IR spectrometer in conjunction with a Pike GladiATR accessory provided with a germanium crystal.

UV−vis absorption spectra were recorded with a Jasco V-570 UV−vis−near-IR instrument. Emission spectra were acquired on a Spex-Jobin Ivon Fluoromax-2 spectrofluorimeter, equipped with Hamamatsu R3896 tubes. Nanosecond emission lifetimes were measured using a TCSPC apparatus (PicoQuant Picoharp300) equipped with sub-nanosecond LED sources (280−600 nm range; 500−700 ps pulse width) powered with a PicoQuant PDL 800-B variable-pulsed (2.5−40 MHz) power supply. The decays were analyzed by means of PicoQuant FluoFit Global Fluorescence Decay Analysis Software.

Transient absorption experiments based on femtosecond laser photolysis were carried out using two different setups: (1) In Ferrara the measurements were performed using a pump−probe setup based on a Hurricane Ti:sapphire laser system (Spectra-Physics) equipped with a TAPPS-Helios with a detection range between 450 and 800 nm (Ultrafast Systems) transient absorption spectrometer. The excitation pulses (560 nm) were generated with an OPA (Spectra Physics 800 OPA). Probe pulses were obtained by continuum generation on a sapphire plate (useful spectral range: 450−800 nm). Effective time resolution ca. 300 fs, temporal chirp over the white-light 450−750 nm range ca. 200 fs, temporal window of the optical delay stage 0−1000 ps. The time-resolved spectral data were analyzed with the Ultrafast Systems Surface Explorer Pro software. (2) In Erlangen the measurements were carried out using an amplified Ti:sapphire laser system CPA-2111 fs laser (Clark MXR − output: 775 nm, 1 kHz and 150 fs pulse width) using a transient absorption pump−probe detection system equipped with a visible and NIR detector (TAPPS Helios - Ultrafast Systems). The excitation wavelength (420 nm) was generated with an NOPA Plus (Clark MXR); pulse widths <150 fs with an energy of 200 nJ were selected.

Materials. All chemicals were purchased from common commercial suppliers and used without further purification, unless otherwise stated. All the solvents for photophysical measurements were of spectroscopic grade. Deuterated solvents were purchased from CIL. *meso*-Tetraphenylporphyrin (**TPP**) and its zincated derivative **ZnTPP** were prepared as described in the literature.[11] Complexes [*fac*-$Re(CO)_3(dmso\text{-}O)_3](PF_6)$ (**1**), [*fac*-$Re(CO)_3(bpy)(dmso\text{-}O)](PF_6)$ (**2**), and [*fac*-$Re(CO)_3(bpy)(py)](PF_6)$ (**8**) were prepared with the procedures previously described for the analogues bearing the trifluoromethanesulfonate as counterion, see also below.[6,7] 5-[4-(4-Methyl-2,2′-bipyridine-4′-carboxyamidyl)phenyl]-10,15,20-(phenyl)-porphyrin (**TPP-Bpy**) was prepared as previously reported by us.[12]

2-(Octylamino)acetic acid. A dichloromethane solution (100 mL) of benzyl bromoacetate (3 mL, 19.1 mmol) was added dropwise to a dichloromethane (150 mL) solution of *n*-octylamine (9 mL, 54.5 mmol) at 0 °C and stirred overnight. The mixture was extracted with distilled water (6 × 50 mL) and purified by column chromatography on silica gel eluting with petroleum ether/ethyl acetate 9/1. A catalytic amount of Pd/C (10% w/w) was added. The solution was left under stirring overnight under hydrogen atmosphere. The mixture was filtered on Celite, and the solvent was removed *in vacuo* to obtain the product as a white solid. Yield: 1.44 g (40%). ^{1}H NMR (δ, 500 MHz, CD_3OD): 3.49 (s, 2H, H_A), 2.55 (t, J = 7.1 Hz, 2H, H_B), 1.38−1.29 (m, 12H, H_C-H_H), 0.88 (t, J = 7.1 Hz, 3H, CH_3).

***N*-Octyl-2(4-pyridine)-3,4-fulleropyrrolidine ($C_{60}C_8Py$).** A solution of C_{60} (250 mg, 0.350 mmol), pyridine-4-carboxaldehyde (0.21 mL, 1.73 mmol), and 2-(octylamino)acetic acid (130 mg, 0.69 mmol) were dissolved in 200 mL of toluene and stirred at reflux for 25 min, and then the solvent was removed *in vacuo*. The product was purified by column chromatography on silica gel initially eluted with toluene to recover unreacted C_{60} and then with toluene/ethyl acetate 95/5. Yield: 185 mg (55%, the yield is based on C_{60} conversion). ^{1}H NMR (δ, 500 MHz, $CDCl_3$): 8.68 (d, J = 5.3 Hz, 2H, py_a), 7.76 (s, 2H, py_b), 5.13 (d, J = 9.4 Hz, 1H, H_B), 5.05 (s, 1H, H_A), 4.15 (d, J = 9.4 Hz, 1H, $H_{B'}$), 3.16 (dt, J = 11.9, 8.5 Hz, 1H, H_C), 2.59 (ddd, J = 12.4, 8.4, 4.4 Hz, 1H, $H_{C'}$), 2.06−1.82 (m, 2H, H_D), 1.75−1.50 (m, 2H, H_E), 1.50−1.18 (m, 10H, $H_{F\text{-}J}$), 0.92 (t, J = 6.9 Hz, 3H, CH_3). ^{13}C NMR (δ, HSQC, $CDCl_3$): 150.26 ($C_{H\text{-}pya}$), 124.27 ($C_{H\text{-}pyb}$), 81.25 (C_{H-A}), 66.72 (C_{H-B}), 53.16 (C_{H-C}), 31.76 (C_{H-J}), 29.30 ($C_{H-(F-H)}$), 28.18 (C_{H-D}), 27.34 (C_{H-E}), 22.51 (C_{H-I}), 14.01 ($C_{H-(CH3)}$). Selected IR bands (cm^{-1}, solid state): 1054, 1032, and 1012 (s, $\nu_{N-C\ pyrrolidine}$). UV−vis (λ_{max}, nm, CH_2Cl_2): 257, 308, 325, 430. ESI-MS (m/z) (positive mode): calcd for $[M + H]^+$ 953.2, found 953.4.

5-[4-(4-Methyl-2,2′-bipyridine-4′-carboxyamidyl)phenyl]-10,15,20-triphenyl zinc porphyrin (ZnTPP-Bpy). A chloroform solution (25 mL) of **TPP-Bpy** (148 mg, 0.18 mmol) was treated overnight with 2.5 equiv of $Zn(CH_3COO)_2{\cdot}2H_2O$ (99 mg, 0.45 mmol) dissolved in the minimum amount of methanol (3 mL). The

solution was dried *in vacuo*. The product was purified by column chromatography on aluminum oxide eluted with chloroform/*n*-hexane 80/20, and vacuum-dried. Yield: 128.6 mg (81%). ^{1}H NMR (δ, 500 MHz, $CDCl_3$): 8.98 (dt, J = 8.0, 4.0 Hz, 2H, βH), 8.95 (s, 6H, βH), 8.94 (d, J = 4.9 Hz, 1H, $H_{6'}$), 8.91 (s, 1H, $H_{3'}$), 8.62 (d, J = 4.8 Hz, 1H, H_6), 8.50 (s, 1H, NH), 8.37 (s, 1H, H_3), 8.26 (d, J = 8.3 Hz, 2H, oNH), 8.25–8.20 (m, 6H, oH), 8.08 (d, J = 8.1 Hz, 2H, mNH), 7.97 (d, J = 3.4 Hz, 1H, $H_{5'}$), 7.80–7.71 (m, 9H, m+pH), 7.24 (s, 1H, H_5), 2.51 (s, 3H, CH_3). ^{13}C NMR (δ, HSQC, $CDCl_3$): 150.37 ($C_{H\text{-}6'}$), 149.11 ($C_{H\text{-}6}$), 134.62 ($C_{H\text{-}o\text{NH}}$), 134.09 ($C_{H\text{-}o\text{H}}$), 131.80 ($C_{H\text{-}\beta\text{H}}$), 126.95 ($C_{H\text{-}p\text{H}}$), 125.35 ($C_{H\text{-}m\text{H}}$), 122.30 ($C_{H\text{-}3}$), 121.61 ($C_{H\text{-}5'}$), 118.33 ($C_{H\text{-}m\text{NH}}$), 117.19 ($C_{H\text{-}3'}$), 21.24 ($C_{H\text{-}(CH3)}$). UV–vis ($\lambda_{max}$, nm, CH_2Cl_2): 245, 290, 422, 552, 594. ESI-MS (m/z) (negative mode): calcd for $[M - H]^-$ 886.2, found 886.1.

[*fac*-Re(CO)$_3$(dmso-O)$_3$](PF$_6$) (1). [ReBr(CO)$_5$] (0.60 g, 1.48 mmol) was dissolved in a mixture of acetone (30 mL) and dmso (680 μL, 9.6 mmol). $AgPF_6$ (0.38 g, 1.48 mmol) was added, and the light-protected mixture was heated to reflux for 4 h. After removal of AgBr by filtration, the colorless solution was concentrated *in vacuo* to ca. 3 mL and stored at room temperature after dropwise addition of diethyl ether until saturation (precipitation of residual AgBr may occasionally occur upon addition of ether). Colorless crystals formed within a few days and were removed by filtration, washed with diethyl ether, and vacuum-dried. Yield 0.67 g (70%). Anal. Calcd: M_W = 649.60, $C_9H_{18}O_6F_6P_1S_3Re$. Requires: C, 16.6%; H, 2.79%. Found: C, 16.4%; H, 2.72%. ^{1}H NMR (δ, 500 MHz, CD_3NO_2): 2.93 (s, 18H, CH_3 dmso-O). Selected IR bands (cm^{-1}, solid state): 2026 (s, $\nu_{C=O\ fac}$), 1902 and 1871 (s, br, $\nu_{C=O\ fac}$), 950 (s, $\nu_{S=O\ dmso\text{-}O}$), 843 (s, ν_{P-F}), 475 (m, ν_{Re-O}).

[*fac*-Re(CO)$_3$(bpy)(dmso-O)](PF$_6$) (2). **1** (100 mg, 0.15 mmol) and 2,2′-bipyridine (31 mg, 0.2 mmol) were dissolved in acetone (15 mL). The solution, initially almost colorless, was refluxed for 1 h under argon atmosphere and turned yellow. Concentration *in vacuo* to ca.10 mL followed by addition of a few drops of diethyl ether induced the formation of yellow microcrystals, which were removed by filtration, washed with diethyl ether, and vacuum-dried. Yield: 84 mg (85%). Anal. Calcd: M_W = 649.52, $C_{15}H_{14}N_2O_4F_6P_1S_1Re$. Requires: C, 27.7%; H, 2.17%; N, 4.31%. Found: C, 28.1%; H, 2.12%; N, 4.24%. ^{1}H NMR (δ, 500 MHz, CD_3NO_2): 9.15 (d, J = 4.8 Hz, 2H, $H_{6,6'}$), 8.55 (d, J = 8.2 Hz, 2H, $H_{3,3'}$), 8.37 (t, J = 8.1 Hz, 2H, $H_{5,5'}$), 7.80 (t, J = 8.1, 2H, $H_{4,4'}$), 2.62 (s, 6H, CH_3 dmso-O). Selected IR bands (cm^{-1}, solid state): 2032 (s, $\nu_{C=O\ fac}$), 1910 and 1890 (s, br, $\nu_{C=O\ fac}$), 951 (s, $\nu_{S=O\ dmso\text{-}O}$), 842 (s, ν_{P-F}), 485 (m, ν_{Re-O}).

[*fac*-Re(CO)$_3$(bpy)(C$_{60}$C$_8$Py)](PF$_6$) (3). **C$_{60}$C$_8$Py** (50.4 mg, 0.053 mmol) was added to a solution of **2** (44.9 mg, 0.069 mmol) in anhydrous dichloromethane (15 mL). The mixture was stirred at reflux for 24 h. A brown solid was precipitated after concentration *in vacuo* followed by addition of diethyl ether. The solid was filtered and vacuum-dried. Yield: 50 mg (60%). ^{1}H NMR (δ, 500 MHz, $CDCl_3$): 9.07 (d, J = 5.5 Hz, 1H, H_6), 8.99 (d, J = 5.4 Hz, 1H, H_6), 8.71 (d, J = 8.2 Hz, 1H, H_3), 8.67 (d, J = 8.2 Hz, 1H, H_3), 8.27 (t, J = 7.1 Hz, 2H, H_5), 8.19 (d, J = 5.5 Hz, 2H, py_a), 7.81 (d, J = 6.1 Hz, 2H, py_b), 7.72 (t, J = 6.8 Hz, 1H, H_4), 7.65 (t, J = 6.7 Hz, 1H, H_4), 5.06 (d, J = 9.7 Hz, 1H, H_B), 5.04 (s, 1H, H_A), 4.10 (d, J = 9.6 Hz, 1H, $H_{B'}$), 3.01–2.91 (m, 1H, $H_{C'}$), 2.61–2.53 (m, 1H, H_C), 1.95–1.78 (m, 2H, H_D), 1.68–1.55 (m, 2H, H_E), 1.49–1.28 (m, 8H, $H_{F\text{-}J}$), 0.92 (t, J = 7.0 Hz, 3H, CH_3). ^{13}C NMR (δ, HSQC, $CDC1_3$): 152.73 ($C_{H\text{-}6}$), 151.56 ($C_{H\text{-}pya}$), 141.56 ($C_{H\text{-}5}$), 128.70 ($C_{H\text{-}4}$), 127.03 ($C_{H\text{-}pyb}$), 126.13 ($C_{H\text{-}3}$), 80.03 ($C_{H\text{-}A}$), 66.49 (C_{H-B}), 53.49 (C_{H-C}), 31.76 ($C_{H\text{-}J}$), 29.36 ($C_{H\text{-}(F-H)}$), 28.23 ($C_{H\text{-}D}$), 27.51 ($C_{H\text{-}E}$), 22.57 (C_{H-I}), 14.04 ($C_{H\text{-}(CH3)}$). Selected IR bands (cm^{-1}, solid state): 2032 (s, $\nu_{C=O\ fac}$), 1918 (s, br, $\nu_{C=O\ fac}$), 842 (s, ν_{P-F}). UV–vis (λ_{max}, nm, CH_2Cl_2): 254, 313. ESI-MS (m/z) (positive mode): calcd for $[M - PF_6]^+$ 1379.2, found 1379.2.

[*fac*-Re(CO)$_3$(TPP-Bpy)(dmso-O)](PF$_6$) (4). TPP-Bpy (75 mg, 0.092 mmol) and **1** (45 mg, 0.070 mmol) were dissolved in chloroform (15 mL). The mixture was stirred at reflux for 4 h under argon. The purple product was collected by filtration after concentration of the solution and addition of diethyl ether and vacuum-dried. Yield: 60 mg (60%). ^{1}H NMR (δ, 500 MHz, dmso-d_6): 11.29 (s, 1H, NH), 9.38 (d, J = 5.5 Hz, 1H, $H_{6'}$), 9.30 (s, 1H, $H_{3'}$), 9.03 (d, J = 5.7 Hz, 1H, H_6), 8.95 (s, 1H, H_3), 8.93–8.76 (m, 8H, βH), 8.35 (d, J = 5.6 Hz, 1H, $H_{5'}$), 8.33–8.26 (m, 4H, o+mNH), 8.26–8.19 (m, 6H, oH), 7.90–7.81 (m, 9H, m+pH), 7.77 (d, J = 5.4 Hz, 1H, H_5), 2.67 (s, 3H, CH_3), 2.54 (s, 6H, CH_3 dmso-O), −2.90 (s, 2H, -NH). ^{1}H NMR (δ, 500 MHz, $CDCl_3$): 9.44 (s, 1H, NH_{am}), 9.16 (d, J = 5.6 Hz, 1H, $H_{6'}$), 8.96–8.84 (m, 9H, βH+$H_{3'}$), 8.83 (d, J = 5.6 Hz, 1H, H_6), 8.50 (s, 1H, H_3), 8.30 (d, J = 6.2 Hz, 1H, $H_{5'}$) 8.28 (d, J = 3.2 Hz, 4H, o+mNH), 8.26–8.20 (m, 6H, oH), 7.84–7.72 (m, 9H, m+pH), 7.47 (d, J = 6.2 Hz, 1H, H_5), 2.71 (s, 3H, CH_3), 2.60 (d, J = 3.9 Hz, 6H, CH_3 dmso-O), −2.59 (s, 2H, -NH). ^{13}C NMR (δ, HSQC, $CDCl_3$): 153.40 ($C_{H\text{-}6'}$), 151.78 ($C_{H\text{-}6}$), 135.13 ($C_{H\text{-}m\text{NH}}$), 134.51 ($C_{H\text{-}o\text{H}}$), 128.50 ($C_{H\text{-}5}$), 126.86 ($C_{H\text{-}(m+p\text{H})}$), 126.57 ($C_{H\text{-}3,5'}$), 122.01 ($C_{H\text{-}\beta\text{H}}$), 118.82 ($C_{H\text{-}o\text{NH}}$), 38.35 ($C_{H\text{-}(CH3\text{-}dmso)}$), 21.74 ($C_{H\text{-}(CH3)}$). Selected IR bands ($cm^{-1}$, solid state): 2030 (s, $\nu_{C=O\ fac}$), 1918 (s, br, $\nu_{C=O\ fac}$),, 1677 (m, $\nu_{C=O}$), 966 (m, $\nu_{S=O\ dmso\text{-}O}$), 842 (s, ν_{P-F}). UV–vis (λ_{max}, nm, CH_2Cl_2): 245, 290, 422, 552, 594. ESI-MS (m/z) (positive mode): calcd for $[M - PF_6 - dmso\text{-}O]^+$ 1096.3, found 1096.2.

[*fac*-Re(CO)$_3$(ZnTPP-Bpy)(dmso-O)](PF$_6$) (5). ZnTPP-Bpy (119 mg, 0.134 mmol) and **1** (79 mg, 0.121 mmol) were dissolved in chloroform (50 mL). The mixture was stirred at reflux for 4 h under argon. The product was collected by filtration after precipitation from a concentrated solution with the addition of diethyl ether and vacuum-dried. Yield: 125 mg (75%). ^{1}H NMR (δ, 500 MHz, $CDCl_3$): 9.30 (s, 1H, NH), 9.06 (d, J = 5.4 Hz, 1H, $H_{6'}$), 8.97 (dd, J = 10.8, 4.5 Hz, 4H, βH), 8.93 (s, 4H, βH), 8.82 (d, J = 5.6 Hz, 1H, H_6), 8.71 (s, 1H, $H_{3'}$), 8.44 (s, 1H, H_3), 8.27–8.22 (m, 6H, oH), 8.20 (d, J = 7.9 Hz, 2H, oNH), 7.97 (d, J = 7.7 Hz, 2H, mNH), 7.82–7.70 (m, 10H, m+pH + $H_{5'}$), 7.47 (d, J = 5.3 Hz, 1H, H_5), 2.71 (s, 3H, CH_3), 2.55 (s, 6H, CH_3 dmso-O). ^{13}C NMR (δ, HSQC, $CDCl_3$): 152.92 ($C_{H\text{-}6'}$), 151.81 ($C_{H\text{-}6}$), 134.65 ($C_{H\text{-}o\text{NH}}$), 134.41 ($C_{H\text{-}o\text{H}}$), 131.96 ($C_{H\text{-}\beta\text{H}}$), 128.55 ($C_{H\text{-}5}$), 127.64 ($C_{H\text{-}5'}$), 127.30 ($C_{H\text{-}(m+p\text{H})}$), 126.10 ($C_{H\text{-}3}$), 121.67 ($C_{H\text{-}3'}$), 118.26 ($C_{H\text{-}m\text{NH}}$), 38.25 ($C_{H\text{-}(CH3\text{-}dmso)}$), 21.65 ($C_{H\text{-}(CH3)}$). Selected IR bands ($cm^{-1}$, solid state): 2030 (s, $\nu_{C=O\ fac}$), 1913 (s, br, $\nu_{C=O\ fac}$), 1670 (m, $\nu_{C=O}$), 950 (m, $\nu_{S=O\ dmso\text{-}O}$), 843 (s, br, ν_{P-F}). UV–vis (λ_{max}, nm, CH_2Cl_2): 245, 300, 423, 552, 595. ESI-MS (m/z) (positive mode) for $[M - PF_6 - dmso\text{-}O]^+$ 1158.2, found 1158.2.

[*fac*-Re(CO)$_3$(TPP-Bpy)(C$_{60}$C$_8$Py)](PF$_6$) (6). **4** (49 mg, 0.037 mmol) and **C$_{60}$C$_8$Py** (36 mg, 0.037 mmol) were dissolved in 1,2-dichloroethane (15 mL). The mixture was stirred at reflux for 24 h under argon. The solution was concentrated *in vacuo* to ca. 10 mL, and the same amount of diethyl ether was added to induce precipitation. A brown pure product was collected by filtration and vacuum-dried. Yield: 57 mg (70%). ^{1}H NMR (δ, 500 MHz, dmso-d_6): 10.88 (s, 1H, NH), 10.75 (s, 1H, NH), 9.51–9.45 (m, 1H, $H_{6'}$), 9.21–9.15 (m, 1H, H_6), 8.90–8.74 (m, 9H, βH+$H_{3'}$), 8.71 (s, 1H, $H_{3'}$), 8.40 (d, J = 6.0 Hz, 2H, py_a), 8.33 (s, 1H, H_3), 8.29 (d, J = 5.9 Hz, 1H, $H_{5'}$), 8.26–8.13 (m, 8H, oH+H_3+$H_{5'}$), 8.10 (d, J = 8.0 Hz, 2H, oNH), 8.02 (d, J = 8.3 Hz, 2H, mNH), 7.93–7.81 (m, 9H, m+pH), 7.78 (d, J = 5.9 Hz, 1H, H_5), 7.70 (d, J = 5.9 Hz, 1H, H_5), 7.63 (d, J = 4.7 Hz, 2H, py_b), 5.07 (s, 1H, H_A), 5.02 (s, 1H, H_A), 4.73 (d, J = 9.1 Hz, 1H, H_B), 4.51 (d, J = 8.9 Hz, 1H, H_B), 3.82–3.60 (m, 1H, $H_{B'}$), 3.04–2.90 (m, 1H, H_C), 2.59–2.53 (m, 1H, H_C), 2.43–2.32 (m, 3H, CH_3), 1.89–1.68 (m, 1H, H_D), 1.66–1.52 (m, 1H, H_D), 1.49–1.26 (m, 10H, H_E-H_I), 1.02–0.76 (m, 3H, H_J), −2.98 (d, 2H, NH). ^{13}C NMR (δ, HSQC, $CDCl_3$): 134.68 ($C_{H\text{-}(o\text{H}+o\text{NH})}$), 127.74 ($C_{H\text{-}m\text{H}}$), 127.63 ($C_{H\text{-}p\text{H}}$), 119.34 ($C_{H\text{-}m\text{NH}}$), 31.65 ($C_{H-I}$), 29.22 ($C_{H\text{-}(F-H)}$), 27.69 ($C_{H\text{-}E}$), 22.31 ($C_{H-I}$), 21.40 ($C_{H\text{-}(CH3)}$), 14.29 ($C_{H\text{-}J}$). Selected IR bands ($cm^{-1}$, solid state): 2036 (s, $\nu_{C=O\ fac}$), 1940 (s, br, $\nu_{C=O\ fac}$), 1914 (s, br, $\nu_{C=O\ fac}$), 1674 (m, $\nu_{C=O}$), 842 (s, br, ν_{P-F}). UV–vis (λ_{max}, nm, CH_2Cl_2): 256, 310, 325, 419, 516, 552, 591, 647. ESI-MS (m/z) (positive mode): calcd for $[M - PF_6]^+$ 2049.2, found 2049.0.

[*fac*-Re(CO)$_3$(ZnTPP-Bpy)(C$_{60}$C$_8$Py)](PF$_6$) (7). **5** (65 mg, 0.047 mmol) and **C$_{60}$C$_8$Py** (45 mg, 0.047 mmol) were dissolved in 1,2-dichloroethane (10 mL). The mixture was refluxed for 24 h under argon. The brown solid formed during the reaction was collected by filtration and vacuum-dried. Yield: 85 mg (80%). ^{1}H NMR (δ, 500 MHz, $CDCl_3$ + 40 μL of CD_3OD): 9.34–9.14 (m, 1H, $H_{6'}$), 9.01–8.92 (m, 1H, H_6), 8.92–8.72 (m, 9H, βH+$H_{3'}$), 8.57 (s, 1H, $H_{3'}$), 8.35

Scheme 1[a]

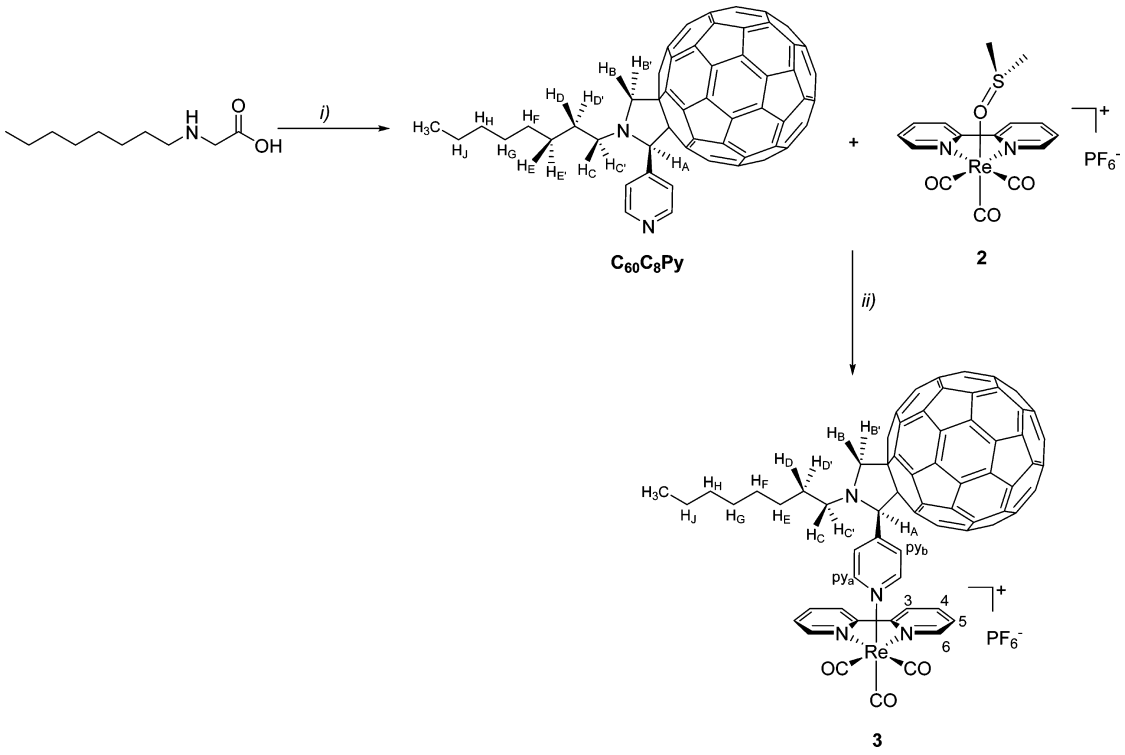

[a](i) C_{60}/pyridine-4-carboxaldehyde, toluene, reflux, 25 min, 55%; (ii) dichloromethane, reflux, 24 h, 60%. For simplicity, only the (*S*) enantiomers are represented for both **$C_{60}C_8$Py** and **3**.

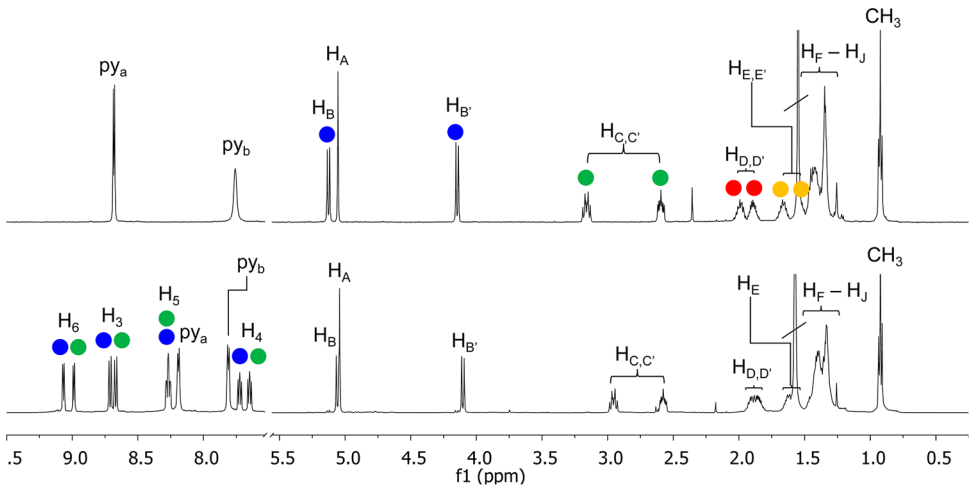

Figure 1. ^{1}H NMR spectra ($CDCl_3$) of **$C_{60}C_8$Py** (above) and **3** (below), with some of the relevant cross peaks from the H–H COSY spectra indicated with circles of the same color; see Scheme 1 for labeling.

(s, 1H, H_3), 8.26–7.94 (m, 13H, *o*H+py_a+(*o*+*m*NH)+$H_{5'}$), 7.80–7.61 (m, 11H, *m*+*p*H+py_b), 7.53–7.39 (m, 2H, H_5), 4.98–4.50 (m, 2H, H_A+H_B), 3.79 (d, *J* = 8.6 Hz, 1H, $H_{B'}$), 3.00–2.87 (m, 1H, H_C), 2.65–2.41 (m, 3H, CH_3), 1.93–1.50 (m, 3H, H_D), 1.48–1.08 (m, 10H, $H_{E\text{-}I}$), 0.92–0.78 (m, 3H, H_J). Selected IR bands (cm^{-1}, solid state): 2036 (s, $\nu_{C=O\ fac}$), 1940 (s, br, $\nu_{C=O\ fac}$), 1914 (s, br, $\nu_{C=O\ fac}$), 1673 (m, $\nu_{C=O}$), 843 (m, ν_{P-F}). UV–vis (λ_{max}, nm, CH_2Cl_2): 258, 313, 326, 422, 553, 593. ESI-MS (*m*/*z*) (positive mode) for $[M - PF_6]^+$ calcd 2112.6, found 2111.5.

[*fac*-Re(CO)$_3$(bpy)(py)](PF$_6$) (8). **2** (30 mg, 0.046 mmol) was dissolved in CH_2Cl_2 (15 mL). After addition of pyridine (37 μL, 0.46 mmol), the solution was stored at ambient temperature for 2 d and then concentrated *in vacuo* to ca. 5 mL. Yellow microcrystals of the product formed upon addition of few drops of diethyl ether and were removed by filtration, washed with diethyl ether, and vacuum-dried. Yield: 22 mg (73%). ^{1}H NMR (δ, 500 MHz, CD_3NO_2): 9.32 (d, *J* = 4.8 Hz, 2H, $H_{6,6'}$), 8.44 (d, *J* = 8.2 Hz, 2H, $H_{3,3'}$), 8.36 (m, 4H, $H_{4,4'}$ + py_a), 7.87 (m, 3H, $H_{5,5'}$ + py_c), 7.35 (t, *J* = 7.1 Hz, 2H, py_b). Selected IR bands (cm^{-1}, solid state): 2026 (s, $\nu_{C=O\ fac}$), 1921 and 1907 (s, br, $\nu_{C=O\ fac}$), 843 (s, ν_{P-F}).

RESULTS AND DISCUSSION

Synthesis and Characterization. The fulleropyrrolidine monoadduct **$C_{60}C_8$Py**, equipped with both a pyridyl group for coordination to the Re(I) metal center and a C_8 alkyl chain to foster solubility, was prepared with the well-known 1,3-dipolar cycloaddition to C_{60} of azomethine ylide, formed from the

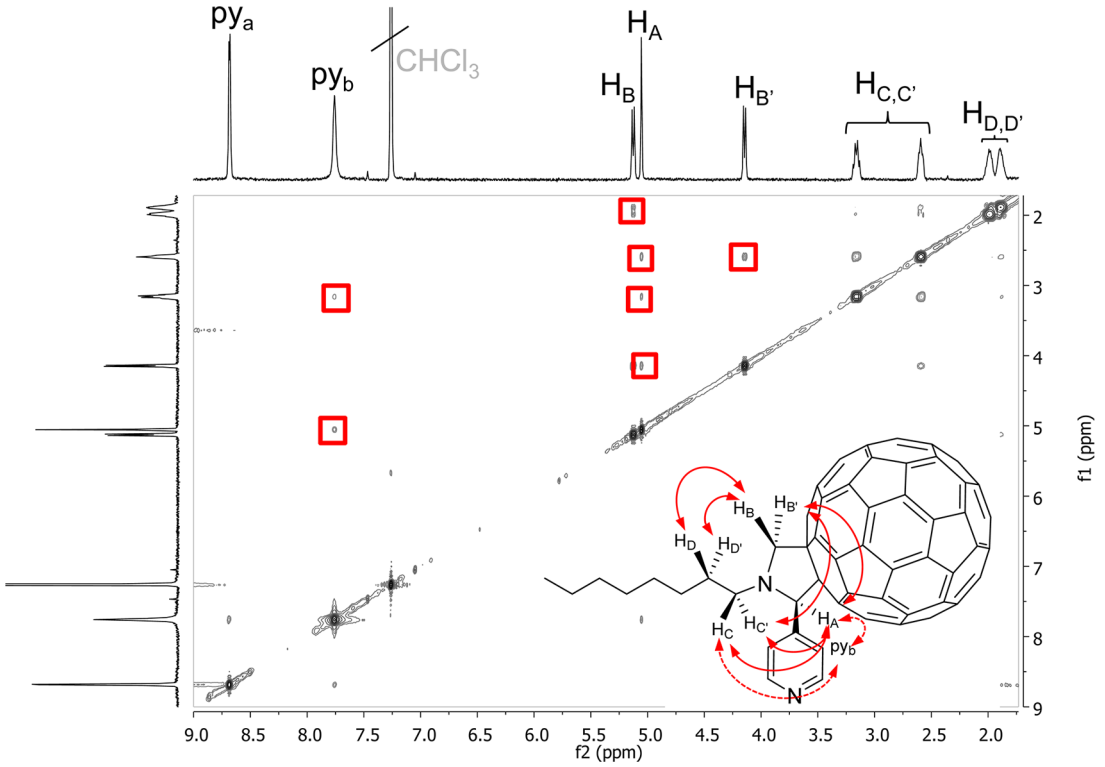

Figure 2. Partial H−H NOESY spectrum ($CDCl_3$) of $C_{60}C_8Py$ with some of the relevant spatial correlations and corresponding NOE cross peaks indicated by arrows and squares, respectively.

Scheme 2[a]

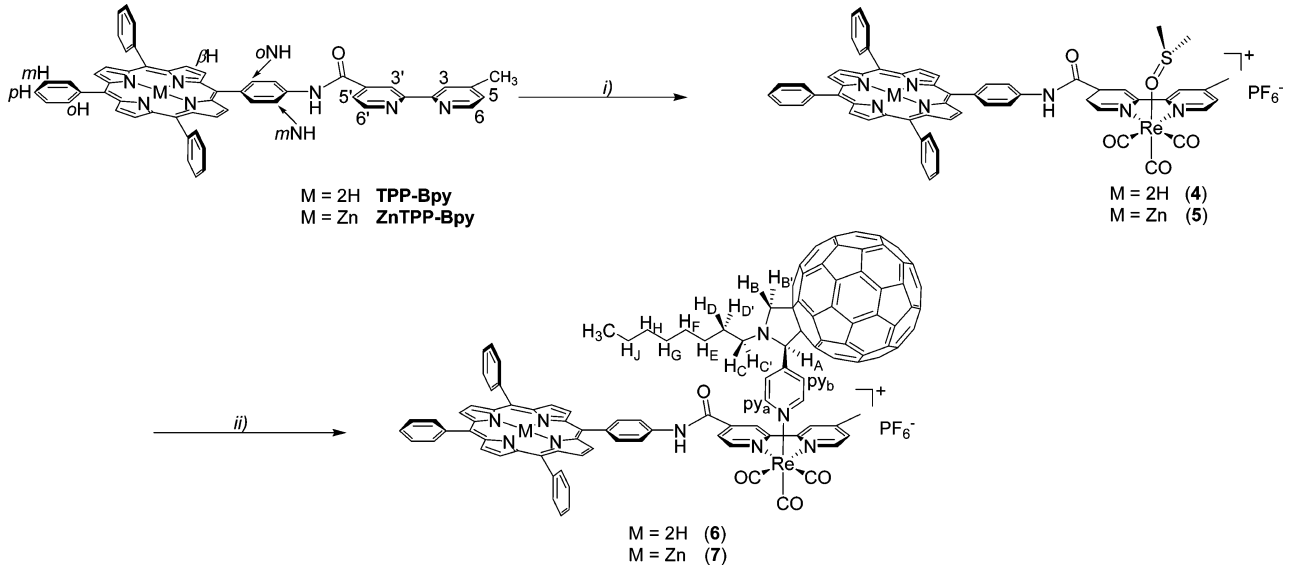

[a](i) **1**, $CHCl_3$, reflux under Ar, 4 h, 70% (**4**) and 75% (**5**); (ii) 1,2-dichloroethane, reflux under Ar, 24 h, 70% (**6**) and 80% (**7**).

condensation of pyridine-4-carboxaldehyde and 2-(octylamino)acetic acid (Scheme 1).[13]

The nonselective generation of a chiral center (carbon $C_{H\text{-}A}$ of the pyrrolidine) is very well-revealed in the ^1H NMR ($CDCl_3$) of $C_{60}C_8Py$. In fact, the geminal protons of the pyrrolidine and of the alkyl chain are diastereotopic and give rise to two sets of resonances, more resolved for the protons closer to the stereogenic center, which can be correctly assigned through the cross peak correlations found in the 2D H−H COSY and NOESY spectra (Figures 1 and 2).

To explore the reactivity of $C_{60}C_8Py$ toward the Re(I) center, and to get useful insights for the characterization of the following target three-component system, the model compound **3** was synthesized (Scheme 1). **3**, obtained in good yield by treatment of [*fac*-$Re(CO)_3$(bpy)(dmso-O)](PF_6) (**2**) with $C_{60}C_8Py$, is well-soluble in chlorinated solvents, and has been fully characterized in solution by ESI mass spectrometry and NMR spectroscopy and in the solid state by IR spectroscopy (see also Figures 6S−9S). In Figure 1 the ^1H NMR ($CDCl_3$) of **3**, which shows the correct relative signal integrations, is

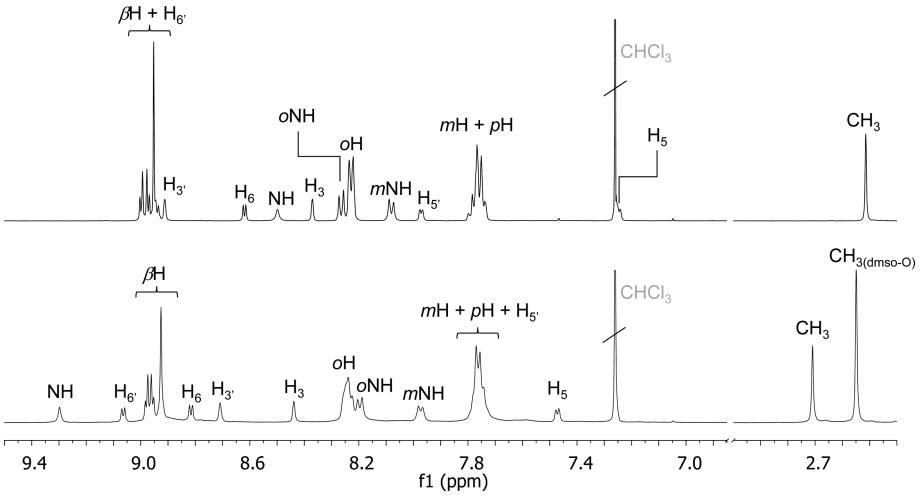

Figure 3. ^{1}H NMR spectra ($CDCl_3$) of **ZnTPP-Bpy** (above) and **5** (below), see Scheme 2 for labeling.

reported; all the assignments were done by means of 2D NMR experiments (H−H COSY, H−C HSQC, and H−H NOESY). The chemical shifts and pattern of the proton resonances of **3** are not particularly affected by its coordination to the {*fac*-$Re(CO)_3$(bpy)} fragment, with the exception of the doublet related to the two pyridyl protons py_a, which is upfield-shifted as a consequence of the mutual perpendicular disposition of the pyridyl and bipyridyl rings ($\Delta\delta$ = −0.45 ppm).[6,7] On the other hand, the presence of a chiral center on the apical fulleropyrrolidine affects the pattern of the proton resonances of the bpy ligand, which loses its orthogonal mirror plane, and thus presents two nonequivalent halves. Two sets of resolved resonances of equal intensities for the bipyridyl protons can be detected, each set pertaining to one of the nonequivalent bpy halves (the two doublets of the H_5 protons are partly collapsed), and presenting its own spin system as revealed in the 2D H−H COSY spectrum (indicated with the blue/green color code in Figure 1).

The target three-component system [*fac*-$Re(CO)_3$(ZnTPP-Bpy)($C_{60}C_8$Py)](PF_6) (**7**) and its free-base analogue [*fac*-$Re(CO)_3$(TPP-Bpy)($C_{60}C_8$Py)](PF_6) (**6**) were both efficiently synthesized via the modular approach already reported by us for the obtainment of (zinc)porphyrin−$Re(CO)_3$(bpy) dyads,[7] and is illustrated in Scheme 2.

Initially, **TPP-Bpy** or **ZnTPP-Bpy**, prepared as previously reported,[12] was reacted with *fac*-[$Re(CO)_3$(dmso-O)$_3$](PF_6) (**1**), in mild conditions and short reaction times, to give the intermediates **4** or **5**, respectively, in very good isolated yields (Scheme 2). These derivatives were fully characterized in solution by ESI mass spectrometry, NMR, UV−vis spectroscopies, and in the solid state by IR spectroscopy (see also Figures 11S-16S). In Figure 3 a comparison between the ^{1}H NMR spectra ($CDCl_3$) of **ZnTPP-Bpy** and **5** is reported. All the proton resonances, and in particular those pertaining to the bipyridyl and the bridging phenyl, were correctly assigned by means of a combination of H−H COSY and 1D NOESY NMR experiments (particularly useful are the long-range correlations between the bpy CH_3 and the H_3/H_5 signals, and the negative Overhauser effects on the resonances of the bpy $H_{3'}$ and the bridging phenyl *m*NH, detected by saturation of the amide NH broad singlet, Figure 16S). Coordination of the **ZnTPP-Bpy** to the metal center induces a downfield shift of most of the bpy chelating moiety ($\Delta\delta$ = 0.25 ÷ 0.12 ppm) and of the amide (NH, $\Delta\delta$ = 0.80 ppm) proton resonances, while the signals of the zinc-porphyrin fragment are substantially unchanged. Very similar features are also observed for **4** (Figures 12S and 13S).

Both **4** and **5** are very valuable intermediates, as they can allow for the relatively *facile* preparation of a potentially infinite variety of three-component systems. In fact, the residual apical dmso-O is labile and may be easily replaced with any chosen photoactive additional partner, provided that this latter is equipped with a donor pyridyl moiety apt for coordination.

From a structural viewpoint, **4** and **5** both exist as mixtures of enantiomers. In fact, the arrangement of the ancillary ligands around rhenium center is, for both species, inherently asymmetrical, and of the type *fac*-$Re(D)_3(C)(B\hat{}A)$, thus identifying one pair of clockwise (C) and anticlockwise (A) enantiomers (Figure 4), most presumably forming in equal amounts.

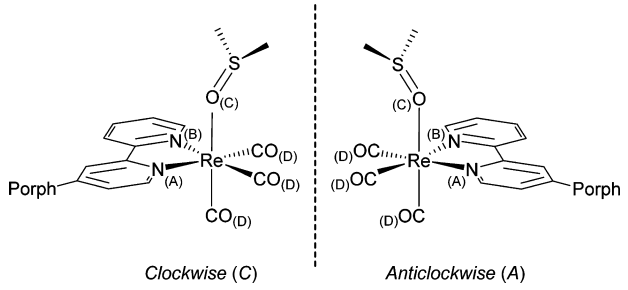

Figure 4. Two mirror images that can be schematically depicted for **4** and **5**.

In the present study, replacement of the apical dmso in **5** (or in **4**) with **$C_{60}C_8$Py**, by refluxing the reactants in 1,2-dichloroethane for ∼24 h, led to the isolation, in very good yield, of the desired three-component system **7** (or of its free-base analogue **6**, Scheme 2). The nature of these products was confirmed by their ESI mass spectra, both presenting a single peak with the correct isotopic distributions for the molecular ion (Figure 5).

The IR spectra (solid state) of both **6** and **7** are consistent with the presence of the *fac*-{$Re(CO)_3$} fragment, as they both present three intense stretching bands: the ones at 1915 and 1940 cm^{-1} are assigned to the CO asymmetric stretching mode, and the one at 2035 cm^{-1} is assigned to the CO symmetric

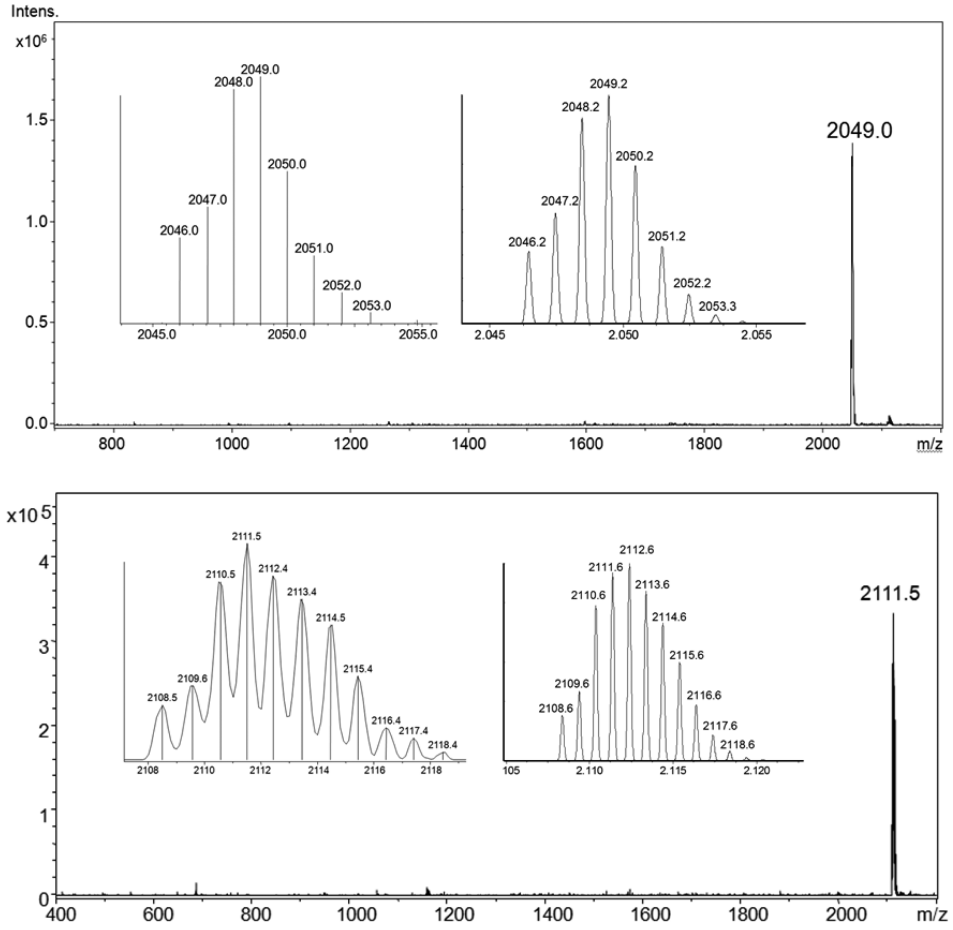

Figure 5. ESI-MS spectra of **6** (above) and **7** (below), with magnifications of the molecular ion peak distributions (experimental left, and calculated—program *IsoPro*—right, respectively).

stretching mode (an additional weak band at 1674 cm^{-1} is assigned to the stretching of the amide CO, Figure 17S).

Given the presence of two stereogenic centers, **6** and **7** both may form mixtures of isomers, and in particular two couples of enantiomers can be structurally drawn, as schematically depicted in Figure 6.

By looking at the possible relative orientations of the (zinc)-porphyrin and the fullerene moieties within the same molecule and with respect to an orthogonal plane bisecting the bpy ligand, the two couples of enantiomers present two distinct situations: one in which the two moieties are located on opposite sides ($Re_{(C)}$,$C_{60(S)}$ and $Re_{(A)}$,$C_{60(R)}$ in Figure 6, top), and the second in which they reside on same sides ($Re_{(C)}$,$C_{60(R)}$ and $Re_{(A)}$,$C_{60(S)}$ in Figure 6, bottom). Accordingly, two distinct proton resonance sets are expected in the ^{1}H NMR spectra of **6** and **7**. Indeed, a high degree of complexity in terms of number of resonances and extended overlaps, which made a correct interpretation quite troublesome, was found in their NMR spectra. We believe that the main spectroscopic features are worth a brief discussion, as they may prove valuable for the characterization of other conjugates of a similar type. A spectrum (dmso-d_6) of **6** is reported in Figure 7, with assignments achieved by means of 1D and 2D NMR experiments (the alkyl resonances region has been omitted, for clarity).

Two sets of signals, more or less resolved, can be observed for both the **TPP-Bpy** and the **C_{60}C$_8$Py** ligands attached to the *fac*-Re(CO)$_3$ fragment. This observation is particularly evident for the resonances of protons NH of the amide; $H_{6'}$, H_6, and H_5 of the bpy fragment; H_A and H_B of the fulleropyrrolidine, and the −NH of the porphyrin unit (Figure 7). An analogous pattern can be revealed by H−H COSY for the resonances of the $H_{5'}$ bpy proton, presenting two distinct correlation peaks with those of $H_{6'}$ (Figure 19S). The two resonances arising from H_3/$H_{3'}$ bpy protons were assigned thanks to their NOE correlations with the amide NH broad singlets, and long-range COSY correlations with the $-CH_3$ bpy protons, respectively (Figures 20S and 21S). Apparently, the relative intensity of the two proton sets is not equal, which may be an indication that the product contains different amounts of the possible isomers.[14–16] Nevertheless, by varying the NMR solvent, the ratio of the two resonance sets is also found to be varied, and in particular when the product is completely dissolved, an almost one-to-one ratio is observed (the ^{1}H NMR of **6** in DMF-d_6, with only some relevant proton resonances, as most of the other signals overlap and/or are hidden below the residual DMF, is reported in Figure 8).

The zincated three-component target triad **7** shows a limited solubility in chlorinated solvents and precipitates during the reaction progress. The solubility of the isolated product is also poor in the other common organic solvents. If methanol, that axially binds to the zinc ion, thus interfering with the π,π intermolecular interactions between zinc-porphyrin macrocycles, and/or zinc-porphyrin and fullerene aromatic surfaces, is added to suspensions of **7** in chloroform, a significant increase of solubility is obtained. Still, only a partial assignment

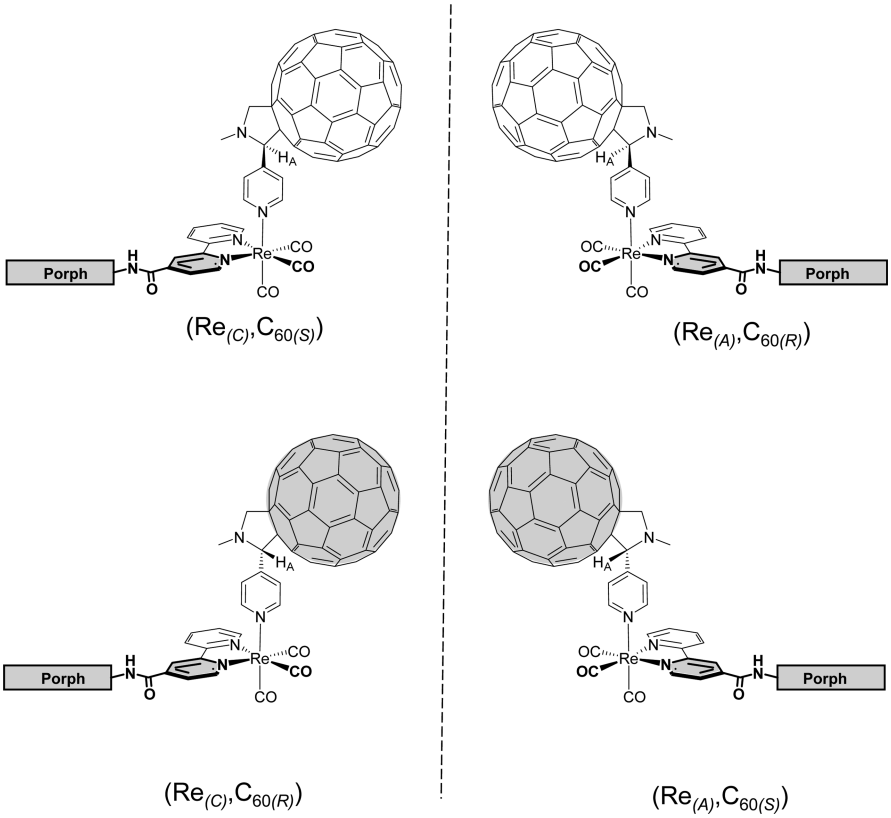

Figure 6. Depiction of the possible isomers of **6** and **7**, constituted by two couples of enantiomers, arising from the presence of two stereocenters.

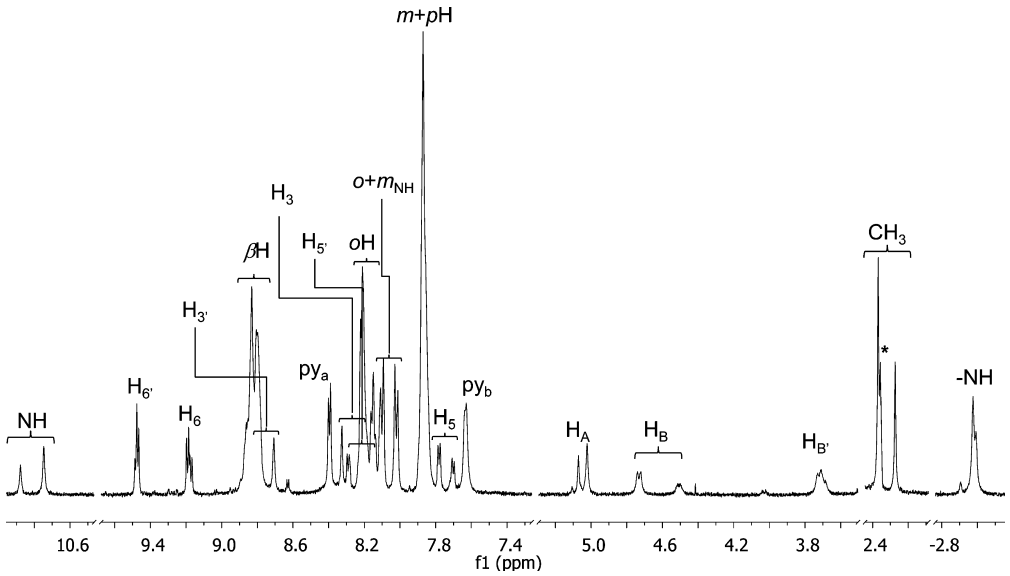

Figure 7. ^{1}H NMR spectrum (dmso-d_6) of **6**, see Scheme 2 for labeling (the asterisk indicate a satellite of the residual dmso).

of the resonances of the ^{1}H NMR spectrum was possible (Figure 22S), with most of it derived from a combination of H−H COSY and NOESY spectra, and also by comparison with the free-base analogue **6** just described. In particular, at least four sets of resolved resonances appear distinctly for some of the protons, most propably as a consequence of the partial coordination of methanol to the zinc, that produces a larger distribution of isomeric species.[14−16]

Photophysical Characterization of the Triad 7.[17] The absorption spectrum of **7** in dichloromethane (Figure 23S) is, besides some very minor shifts (∼2−3 nm), best described as the superimposition of the absorption of the corresponding model compounds. This fact indicates that there are only very weak interactions between the individual components in the ground state. The absorption spectrum of compound **7** is dominated by the Soret band (around 430 nm) and the two Q bands (between 500 and 700 nm) of the ZnP moiety. Compared to ZnP, the rhenium complex and the fullerene are predominantly absorbing light in the UV region (Figure 23S).

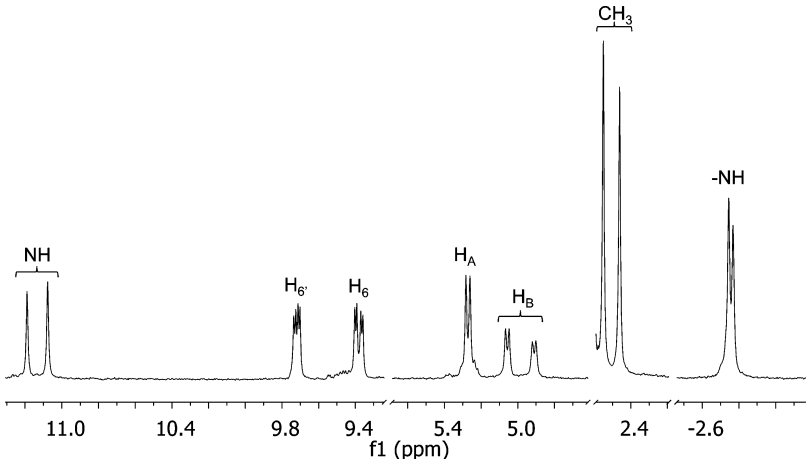

Figure 8. Partial ^{1}H NMR spectrum (DMF-d_6) of **6**, see Scheme 2 for labeling.

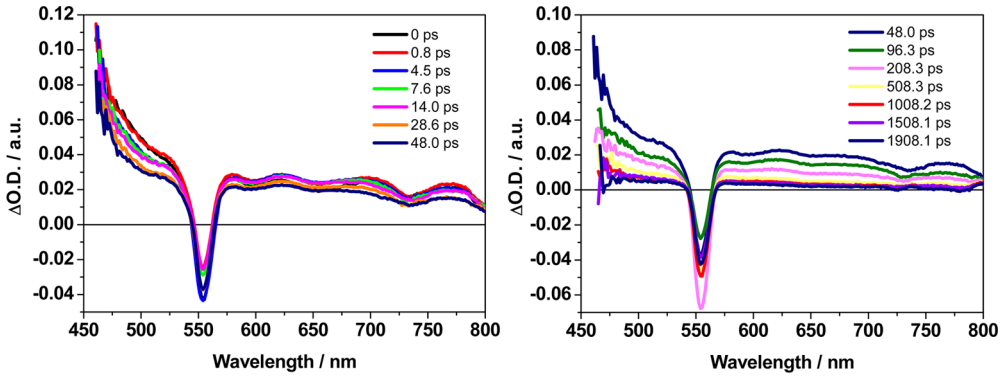

Figure 9. Transient absorption spectra obtained for **7** in a DCM solution (λ_{exc} = 560 nm) in the 0−10 ps range (left) and in the 50−2000 ps range (right).

Taking the former into account, an exclusive excitation of the ZnP chromophore is feasible in the visible region of the spectrum. A detailed photophysical investigation of the new triad was carried out in dichloromethane solution, upon visible excitation, by steady state and time-resolved absorption and emission spectroscopy. At room temperature, a solution of the triad shows the typical Zn-porphyrin fluorescence with prominent vibronic bands at 599 and 648 nm (Figure 24S); even taking a close look into the 700−750 region, no C_{60}-centered fluorescence was observed, neither in DCM nor in less polar solvents (e.g., toluene). Comparative experiments, carried out on optically matched solutions of **7** and the **ZnTPP** model at λ_{exc} = 516 nm, indicate that, in the triad, the zinc-porphyrin fluorescence, although maintaining the same emission pattern, is strongly quenched relative to that of the model compound ($\Phi_0/\Phi \geq 100$, where Φ_0 and Φ are the fluorescence quantum yields of the **ZnTTP** model and **7**, respectively, Figure 24S). Single-photon counting experiments demonstrate that the fluorescence lifetime of the ZnP−Re−C_{60} triad **7** lies below the instrumental time resolution (<250 ps). To obtain insight into the quenching mechanism, ultrafast transient absorption experiments were performed in different solvents (dichloromethane, toluene, benzonitrile, and tetrahydrofuran) and with different experimental setups and excitation wavelengths.

The transient absorption spectra observed in dichloromethane upon excitation at 560 nm are shown in Figure 9. The initial spectrum, taken immediately after the excitation pulse ($\tau \approx 1$ ps), is identical with the transient absorption spectrum typically observed for the zinc-porphyrin singlet excited state, characterized by a broad intense positive absorption in the 450−550 nm range, a relatively flat positive absorption in the visible region in the 560−800 nm range with superimposed transient bleaching of the ground-state Q bands (580−600 nm). Additional apparent bleaches in the 650−720 nm range are caused by stimulated emission.

The transient spectral changes show a biphasic behavior, taking place in the 1−50 ps and in the 50−2000 ps range (Figure 9). In the first range a fast increase of the optical density in the 620−700 nm range and a reduction of Q-band bleach are observed. These spectral changes are relatively small, but the signatures of the radical cation of the zinc-porphyrin component (broad absorption bands in the 600−800 nm range) can be easily recognized, consistent with the formation of a charge-separated state in which this component is oxidized (ZnP^+).[18] In the longer time range (50−2000 ps) a uniform decay of ZnP^+ spectrum toward the initial baseline is observed, clearly indicating that ZnP^+ converts quantitatively to the ground state. These results are consistent with an electron-transfer mechanism for the quenching of excited singlet state of the ZnP component. Kinetic analysis of the spectral changes at 650 nm (Figure 25S) yields a time constant of 2 ± 1 ps for the first process (formation of ZnP^+) and 140 ± 10 ps for the second one (conversion to ground state).

In these measurements, the investigated spectral window (400−800 nm) is limited by experimental setup (see Experimental Section). To obtain evidence on the nature of

the charge separated state it is necessary to extend the study to the infrared region, in which the C_{60}^{-} shows its transient absorptions. For this purpose, a transient absorption detection system with a wider spectral window (400−1200 nm) was employed. Experiments in various solvents (toluene, THF, and benzonitrile), by using 420 nm as excitation wavelength, were performed (see also Figures 26S and 27S).[19] The spectral changes observed in toluene are reported in Figure 10.

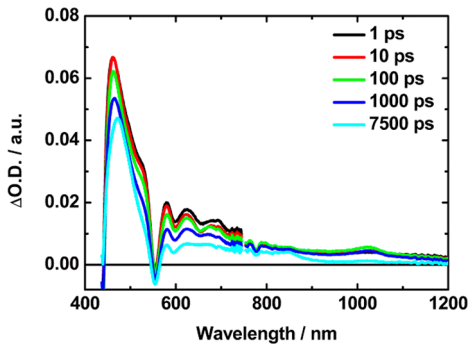

Figure 10. Femtosecond transient absorption spectra of **7** in argon-saturated toluene, after excitation at 420 nm.

Immediately after excitation of the ZnP component (τ = 0.1 ps), its singlet excited state is formed. Evidences for the latter stem from the occurrence of an intense absorption with maxima at 462, 570, and 615 nm as well as minima at 550, 600, and 620 nm corresponding to the bleach of the ground-state Q bands and to the stimulated emission. In the early time scale (0−30 ps), spectral changes with signatures of radical cation ZnP^{+} (maxima at 460, 625, and 675 nm and a minimum at 555 nm) and a maximum at 1025 nm, which corresponds to the typical absorption of the radical anion, C_{60}^{-}, are clearly discernible. These observations indicate that a charge-separated product (ZnP^{+}−Re−C_{60}^{-}), in which the zinc-porphyrin chromophore is oxidized and the fullerene unit is reduced, is formed. Importantly, the ZnP^{+}−Re−C_{60}^{-} features grow in a time scale that matches the decay of the ZnP singlet excited state, indicating that a photoinduced electron-transfer process from the ZnP excited state to C_{60} component occurs. In a longer time scale, the spectroscopic signatures of the charge-separated state, ZnP^{+}−Re−C_{60}^{-}, disappear with a decay of the whole spectrum toward the initial baseline. The transient changes show that, in THF and benzonitrile, ZnP^{+}−Re−C_{60}^{-} converts by charge recombination to the ground state (Figures 30S and 31S), whereas in toluene (Figures 28S and 29S), the recombination process is much slower (see Table 1), the charge-separated state ZnP^{+}−Re−C_{60}^{-} undergoes spin inversion and yields the Zn porphyrin triplet state upon charge recombination.[20]

Table 1. Time Constants (τ) for the Charge Recombination Process in Different Solvents

solvent	ε^{a}	τ (ps)
benzonitrile	25.7	125
DCM	9.1	140
THF	7.6	260
toluene	2.4	2800

[a] ε is the dielectric constant.

Kinetic analysis of the spectral changes observed in the different solvents indicates that, while the charge-separation process is very fast (1−2 ps) and nearly independent of the polarity of the solvent, the charge recombination, leading to the ground state, is by far slower and strongly solvent dependent. The values of the time constants of the charge recombination process reported in Table 1 are obtained from kinetics analyses at three different wavelengths: 650, 465, 1020 nm (see also Figures 28S−31S).

In conclusion, the interpretation of the transient spectral changes observed in the ultrafast absorption experiments as formation and decay of the charge-separated product ZnP^{+}−Re−C_{60}^{-}, respectively, is straightforward. In all solvents investigated no evidence of an intermediate species ZnP^{+}−Re^{-}−C_{60}, where the ZnP is oxidized and rhenium component is reduced, was obtained. To discuss this point, it is useful consider a simplified energy level diagram for **7** studied in dichloromethane (Figure 11, the excited states of the C_{60} unit are omitted for clarity).[21]

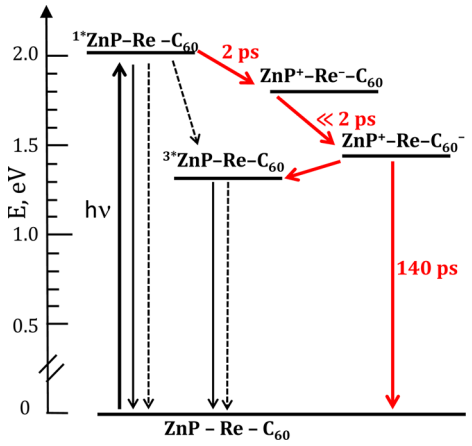

Figure 11. Energy level diagram for **7** and photophysical processes in dichloromethane.

In this diagram, in addition to the energy levels of the excited states of the ZnP chromophore, two types of intercomponent charge transfer states, both containing the oxidized form of the zinc-porphyrin component, must be considered: one, in which the rhenium-based unit is reduced (ZnP^{+}−Re^{-}−C_{60}) and the other, in which the C_{60} unit is reduced (ZnP^{+}−Re−C_{60}^{-}). The energy of these states can be obtained from the measured redox potentials for the three-component system **7** (Table 2) as

Table 2. Electrochemical Data for 7 and for Its Model Compounds[a,b]

compound	$E_{1/2\ (red)}$ (1) (V)	$E_{1/2\ (red)}$ (2) (V)	$E_{1/2\ (ox)}$ (V)
ZnTPP	−1.38[c]		+0.80[c]
8	−1.13[c]		
C_{60}	−0.55[d]		
3	−0.58	−1.00	
7	−0.65	−1.03	+0.77

[a] All measurements were made in N_2-deaerated CH_2Cl_2 solutions at 298 K (0.1 tetrabutylammonium hexafluorophosphate ($TBAPF_6$) as supporting electrolyte); scan rate 100 mV/s; SCE as reference electrode, and glassy carbon as working electrode). [b] Half wave potential in cyclic voltammetry (ΔE_p = 60−80 mV). [c] From ref 7. [d] From ref 9f.

difference in the potentials for oxidation of the Zn-porphyrin unit ($E_{1/2(ox)}$ (ZnP/ZnP^+) = +0.77 V vs SCE) and for the reduction of the rhenium ($E_{1/2(red)}$ (Re/Re^-) = −1.03 V vs SCE) and the C_{60} ($E_{1/2(red)}$ (C_{60}/C_{60}^-) = −0.65 V vs SCE) components, respectively (see also Figure 33S), with appropriate correction for the electrostatic work term. The redox potential values of **7** are very close to those found for the corresponding models **ZnTPP**, C_{60}, **8**, and **3** (Table 2 and Figure 32S), in agreement with the supramolecular nature of **7**.

Within the limits of this type of calculation, the $ZnP^+-Re^--C_{60}$ is estimated to lie at 1.80 eV, and the $ZnP^+-Re-C_{60}^-$ is at 1.42 eV, both lower in energy than the singlet state of the zinc porphyrin [$E(S_1)$ = 2.02 eV] (Figure 11).

$$^{1*}ZnP-Re-C_{60} \rightarrow ZnP^+-Re^--C_{60}\ \Delta G = -0.22eV \quad \text{(eq 1)}$$

$$ZnP^+-Re^--C_{60} \rightarrow ZnP^+-Re-C_{60}^-\ \Delta G = -0.38eV \quad \text{(eq 2)}$$

The charge-separated state, $ZnP^+-Re-C_{60}^-$, recombines to the ground state in a longer time scale (eq 3).

$$ZnP^+-Re-C_{60}^- \rightarrow ZnP-Re-C_{60}\ \Delta G = -1.42\ eV \quad \text{(eq 3)}$$

The kinetics of the processes (eq 1, eq 2, eq 3) can be analyzed in the light of standard electron-transfer theory. In the limit of weak interaction (non-adiabatic regime), the rate constant for an electron-transfer process from a donor to an acceptor is given by the following equation:

$$k = \frac{2\pi}{\hbar} H_{DA}{}^2 FCWD \quad \text{(eq 4)}$$

where H_{DA} is the electronic coupling between donor and acceptor and FCWD is the nuclear term (Franck−Condon weighted density of states) that accounts for the combined effects of the reorganizational energies and driving force. In principle, the fact that the electron-transfer processes (eq 1, eq 2, and eq 3) have different electronic factors as well as different nuclear factors does not allow making a quantitative comparison between the rate constant values experimentally measured. However, some remarkable comments can be useful to rationalize the kinetic data. As far as the charge-separation and charge-shift processes (eq 1 and eq 2) are concerned, since the driving forces of the processes place both in the normal Marcus region (assuming approximately similar reorganizational energies), the charge-shift process (eq 2) is expected to be faster being less activated. Moreover, this process is kinetically favored by the electronic factor: it involves the C_{60} component directly connected to the rhenium unit via the pyridyl group, while, in the case of the photoinduced charge separation process (eq 1), an amido bridge is interposed between ^{1*}ZnP and Re components. Regarding the kinetics of processes 1 and 3, it is worth also pointing out that the rate of the charge recombination (eq 3) to ground state is significantly slower than the charge separation (eq 1) in all investigated solvents. This result can be easily explained by considering that, for process 3, both nuclear (process 3 presumably falls in the Marcus inverted region) and electronic (the electron transfer occurs between two sites not directly connected) factors are less favorable.

As reported above, the data of Table 1 clearly indicate that the kinetics of the charge-recombination process was found to be strongly solvent-dependent, with rate constants decreasing with decreasing solvent polarity. A similar solvent dependence was observed for the charge-recombination process occurring in the previously studied ZnP−Re dyad (see Chart 1) and can be qualitatively explained in terms of Marcus theory as a consequence of the changes in the driving force and reorganizational energy with changing the solvent in the hypothesis that the process belongs to the Marcus inverted region.

Of particular interest to the present work is the comparison with the dyad studied by Perutz, constituted by the same chromophoric (ZnP) and electron-acceptor ({$Re(CO)_3(bpy)$}) components, covalently attached by an amide bridge (Figure 12).[4d,e]

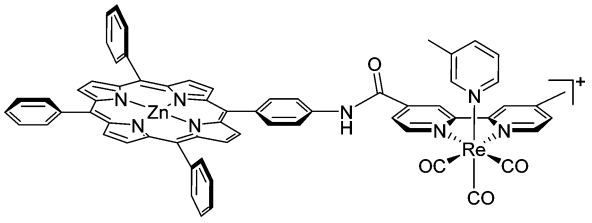

Figure 12. Dyad studied by Perutz.[4d,e]

The rate of photoinduced charge-separation process reported by Perutz is practically the same (a few picoseconds) as we measured in the present study. This fact confirms the hypothesis of a stepwise mechanism for the formation of the charge-separated product $ZnP^+-Re-C_{60}^-$ where the electron transfer from the ZnP first singlet excited state to the rhenium component is the rate-determining step. On the other hand, the result that the charge-recombination process in Perutz system is faster (53 ps vs 260 ps measured in the same solvent, THF) can be explained by considering that, in our system, the charge-recombination process involves two components (ZnP and fullerene unit) that are not directly bound.

A related dyad system constituted by a zinc porphyrin covalently linked to a C_{60} unit has been investigated by Imahori et al. (Figure 13).[9d]

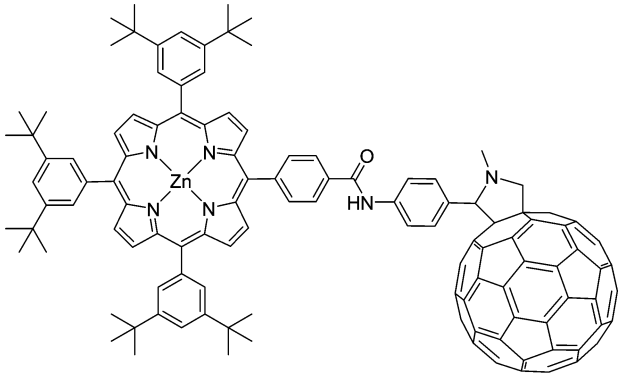

Figure 13. Zinc porphyrin−C_{60} dyad studied by Imahori.[9d]

They found that, in benzonitrile, a photoinduced charge separation from ZnP to fullerene was followed by a recombination process occurring with time constants of 100 and 760 ps, respectively. In our system, the photoinduced process is by far faster (ca. 1 ps), probably because there is a stronger electronic interaction between the components involved in the electron-transfer reaction (the singlet excited

state of ZnP and the bpy ligand of the $\{Re(CO)_3(bpy)\}$ fragment). On the other hand, the rate of 125 ps observed in our case for the charge recombination of the $ZnP^+-Re-C_{60}^-$ state, and faster with respect to that reported by Imahori, may be ascribed to a superexchange interaction involving the state $ZnP^+-Re^--C_{60}$ (Figure 11),[22] relatively close in energy.

CONCLUSIONS

In summary, we have here shown how the *facial* tris-acceptor metal precursor $[Re(CO)_3(dmso\text{-}O)_3]^+$ can be conveniently employed to obtain systems containing an increased number of photoactive partners, that is, triads versus dyads, while maintaining an established synthetic strategy. In the present study, the preparation of a new triad featuring one chromophore and two different electron-acceptor moieties has been presented. Careful attention to the characterization studies of this new adduct, featuring two stereogenic centers, of its model and precursor compounds, with special regard to the NMR features, has been given. We believe that this aspect, often neglected or poorly analyzed, will give a valuable contribution to the structural comprehension of similarly inspired derivatives.

The photophysical behavior of the system, upon visible light excitation, has been thoroughly investigated. Electron-transfer processes were detected and kinetically characterized by using a combination of emission spectroscopy and femtosecond time-resolved transient absorption techniques. An ultrafast (ca. 1 ps) photoinduced electron transfer from the zinc-porphyrin chromophore to the $\{Re(CO)_3(bpy)\}$ fragment occurs, followed by a faster charge shift process to the fullerene unit, not allowing for the accumulation of the $ZnP^+-Re^--C_{60}$ intermediate species. Ultrafast transient absorption techniques in the NIR region show clear evidence for the formation of the charge-separated species $ZnP^+-Re-C_{60}^-$. While the rate of charge separation is practically independent of the polarity of the solvent, the kinetics of recombination process depends on the solvent, in agreement with a Marcus inverted behavior.

Efforts are currently focused on the rational design of alternative three-component photoactive systems, by preparation of suitable electron acceptors capable of coordinating to the $ZnP-Re(I)(CO)_3(bpy)$ intermediate via an appended pyridyl group.

ASSOCIATED CONTENT

Supporting Information

Additional compound characterization (ESI-MS, NMR, IR, UV–vis, fluorescence spectra, transient absorption spectra, time profiles, and CV experiments)

AUTHOR INFORMATION

Corresponding Authors

*E-mail: eiengo@units.it. (E.I.)
*E-mail: idm@unife.it. (M.T.I.)

Funding

Financial support from the Italian MIUR (PRIN Project No. 2010N3T9M4 and FIRB Project No. RBAP11C58Y), from the University of Trieste (FRA2009 and FRA2012), from Fondazione Beneficentia Stiftung, and from Deutsche Forschungsgemeinschaft (Grant No. KA 3491/2–1) is gratefully acknowledged.

Notes

The authors declare no competing financial interest.

ACKNOWLEDGMENTS

We thank Dr. C. Chiorboli (Univ. of Ferrara, Italy) for the time-resolved ultrafast measurements (560 nm excitation) in the visible region and Dr. M. Natali (Univ. of Ferrara, Italy) for the cyclic voltammetry measurements. Prof. D. M. Guldi (Friedrich-Alexander-Universität Erlangen-Nürnberg, Germany) is acknowledged for his support during the photophysical experiments in Erlangen.

REFERENCES

(1) (a) Lewis, N. S.; Nocera, D. G. *Proc. Natl. Acad. Sci. U. S. A.* **2006**, *103*, 15729. (b) Barber, J. *Chem. Soc. Rev.* **2009**, *38*, 185–196. (c) Aratani, N.; Kim, D.; Osuka, A. *Acc. Chem. Res.* **2009**, *42*, 1922–1934. (d) Gust, D.; Moore, T. A.; Moore, A. L. *Acc. Chem. Res.* **2009**, *42*, 1890–1898. (e) Hambourger, M.; Moore, G. F.; Kramer, D. M.; Gust, D.; Moore, A. L.; Moore, T. A. *Chem. Soc. Rev.* **2009**, *38*, 25–35. (f) Frischmann, P. D.; Mahata, K.; Würthner, F. *Chem. Soc. Rev.* **2013**, *42*, 1847–1870. (g) Sartorel, A.; Bonchio, M.; Campagna, S.; Scandola, F. *Chem. Soc. Rev.* **2013**, *42*, 2262–2280. (h) Fukuzumi, S.; Ohkubo, K.; Suenobu, T. *Acc. Chem. Res.* **2014**, *47*, 1455–1464. (i) Karkas, M. D.; Jhonston, E. V.; Verho, O.; Akermark, B. *Acc. Chem. Res.* **2014**, *47*, 100–111.

(2) (a) Morris, A. J.; Meyer, G. J.; Fujita, E. *Acc. Chem. Res.* **2009**, *42*, 1983–1994. (b) Takeda, H.; Ishitani, O. *Coord. Chem. Rev.* **2010**, *254*, 346–354. (c) Windle, C. D.; Perutz, R. N. *Coord. Chem. Rev.* **2012**, *256*, 2562–2570.

(3) (a) Hawecker, J.; Lehn, J.-M.; Ziessel, R. *J. Chem. Soc., Chem. Comm.* **1983**, 536. (b) Hori, H.; Ishihara, J.; Koike, K.; Takeuchi, K.; Ibusuki, T.; Ishitani, O. *J. Photochem. Photobiol., A* **1999**, *120*, 119–124. (c) Takeda, H.; Koike, K.; Inoue, H.; Ishitani, O. *J. Am. Chem. Soc.* **2008**, *130*, 2023–2031. (d) Agarwal, J.; Fujita, E.; Schaefer, H. F.; Muckerman, J. T. *J. Am. Chem. Soc.* **2012**, *134*, 5180–5186. (e) Marimoto, T.; Nishiura, C.; Tanaka, M.; Rohacova, J.; Nakagawa, Y.; Funada, Y.; Koike, K.; Yamamoto, Y.; Shishido, S.; Kojima, T.; Saeki, T.; Ozeki, T.; Ishitani, O. *J. Am. Chem. Soc.* **2013**, *135*, 13266–13269. (f) Tsuyoshi, A.; Nakagawa, Y.; Funada, Y.; Sawa, S.; Takeda, H.; Morimoto, T.; Koike, K.; Ishitani, O. *Inorg. Chem.* **2014**, *53*, 7170–7180.

(4) (a) Sato, S.; Koike, K.; Inoue, H.; Ishitani, O. *Photochem. Photobiol. Sci.* **2007**, *6*, 454–461. (b) Kiyosawa, K.; Shiraishi, N.; Shimada, T.; Masui, D.; Tachibana, H.; Takagi, S.; Ishitani, O.; Tryk, D. A.; Inoue, H. *J. Phys. Chem. C* **2009**, *113*, 11667–11673. (c) Tamaki, Y.; Koike, K.; Morimoto, T.; Ishitani, O. *J. Catal.* **2013**, *304*, 22–28. (d) Gabrielsson, A.; Hartl, F.; Zhang, H.; Lindsay Smith, J. R.; Towrie, M.; Vlcek, A.; Perutz, R. N. *J. Am. Chem. Soc.* **2006**, *128*, 4253–4266. (e) Windle, C. D.; Câmpian, M. V.; Duhme-Klair, A.-K.; Gibson, E. A.; Perutz, R. N.; Schneider, J. *Chem. Commun.* **2012**, *48*, 8189–8191.

(5) (a) Hupp, J. T. *Struct. Bonding (Berlin, Ger.)* **2006**, *121*, 145–165. (b) Boccalon, M.; Iengo, E.; Tecilla, P. *J. Am. Chem. Soc.* **2012**, *134*, 20310–20313. (c) Iengo, E.; Cavigli, P.; Milano, D.; Tecilla, P. *Inorg. Chim. Acta* **2014**, *417*, 59–78.

(6) (a) Casanova, M.; Zangrando, E.; Munini, F.; Iengo, E.; Alessio, E. *Dalton Trans.* **2006**, 5033–5045. (b) Ghirotti, M.; Chiorboli, C.; Indelli, M. T.; Scandola, F.; Casanova, M.; Iengo, E.; Alessio, E. *Inorg. Chim. Acta* **2007**, *360*, 1121–1130. (c) Casanova, M.; Zangrando, E.; Iengo, E.; Alessio, E.; Indelli, M. T.; Scandola, F.; Orlandi, M. *Inorg. Chem.* **2008**, *47*, 10407–10418.

(7) Gatti, T.; Cavigli, P.; Zangrando, E.; Iengo, E.; Chiorboli, C.; Indelli, M. T. *Inorg. Chem.* **2013**, *52*, 3190–3197.

(8) (a) Martín, N.; Sánchez, L.; Illescas, B.; Pérez, I. *Chem. Rev.* **1998**, *98*, 2527–2548. (b) Guldi, D. M.; Prato, M. *Acc. Chem. Res.* **2000**, *33*, 695–703.

(9) To cite some of them: (a) Da Ros, T.; Prato, M.; Guldi, D. M.; Ruzzi, M.; Pasimeni, L. *Chem.—Eur. J.* **2001**, *7*, 816–827. (b) Guldi,

D. M. *Chem. Soc. Rev.* **2002**, *31*, 22−36. (c) Armaroli, N.; Accorsi, G.; Felder, D.; Nierengarten, J.-F. *Chem.—Eur. J.* **2002**, *8*, 2314−2323. (d) Imahori, H. *Org. Biomol. Chem.* **2004**, *2*, 1425−1433. (e) D'Souza, F.; Ito, O. *Coord. Chem. Rev.* **2005**, *249*, 1410−1422. (f) Schuster, D. I.; Li, K.; Guldi, D. M.; Palkar, A.; Echegoyen, L.; Stanisky, C.; Cross, R. J.; Niemi, M.; Tkachenko, N. V.; Lemmetyinen, H. *J. Am. Chem. Soc.* **2007**, *129*, 15973−15982. (g) D'Souza, F.; Ito, O. *Chem. Commun.* **2009**, 4913−4928. (h) Poddutoori, P. K.; Sandanayaka, A. S. D.; Zarrabi, N.; Hasobe, T.; Ito, O.; van der Est, A. *J. Phys. Chem. A* **2011**, *115*, 709−717. (i) Garg, V.; Kodis, G.; Chachisvilis, M.; Hambourger, M.; Moore, A. L.; Moore, T. A.; Gust, D. *J. Am. Chem. Soc.* **2011**, *133*, 2944−2954. (j) Bottari, G.; Trukhina, O.; Ince, M.; Torres, T. *Coord. Chem. Rev.* **2012**, *256*, 2453−2477. (k) Wijesinghe, C. A.; El-Khouly, M. E.; Zandler, M. E.; Fukuzumi, S.; D'Souza, F. *Chem.—Eur. J.* **2013**, *19*, 9629−9638. (l) Fukuzumi, S.; Ohkubo, K. *Dalton Trans.* **2013**, *42*, 15845−15858.

(10) (a) Guldi, D. M.; Maggini, M.; Menna, E.; Scorrano, G.; Ceroni, P.; Marcaccio, M.; Paolucci, F.; Roffia, S. *Chem.—Eur. J.* **2001**, *7*, 1597−1605. (b) Armaroli, N.; Accorsi, G.; Felder, D.; Nierengarten, J.-F. *Chem.—Eur. J.* **2002**, *8*, 2314−2323. (c) Chaignon, F.; Torroba, J.; Blart, E.; Borgström, M.; Hammarström, L.; Odobel, F. *New J. Chem.* **2005**, *29*, 1272−1284. (d) Possamai, G.; Menna, E.; Maggini, M.; Carano, M.; Marcaccio, M.; Paolucci, F.; Guldi, D. M.; Swartz, A. *Photochem. Photobiol. Sci.* **2006**, *5*, 1154−1164. (e) Allen, B. D.; Benniston, A. C.; Harriman, A.; Mallon, L. J.; Pariani, C. *Phys. Chem. Chem. Phys.* **2006**, *8*, 4112−4118. (f) Karlsson, S.; Modin, J.; Becker, H.-C.; Hammarström, L.; Grennberg, H. *Inorg. Chem.* **2008**, *47*, 7286−7294. (g) Iehl, J.; Vartanian, M.; Holler, M.; Nierengarten, J.-F.; Delavaux-Nicot, B.; Strub, J.-M.; Van Dorsselaer, A.; Wu, Y.; Mohanraj, J.; Yoosaf, K.; Armaroli, N. *J. Mater. Chem.* **2011**, *21*, 1562−1573. (h) Walsh, E. A.; Deye, J. R.; Baas, W.; Sullivan, K.; Lancaster, A.; Walters, K. A. *J. Photochem. Photobiol., A* **2013**, *260*, 24−36.

(11) Fleischer, E. B.; Shachter, A. M. *Inorg. Chem.* **1991**, *30*, 3763−3769.

(12) Gianferrara, T.; Bratsos, I.; Iengo, E.; Milani, B.; Ostrić, A.; Spagnul, C.; Zangrando, E.; Alessio, E. *Dalton Trans.* **2009**, 10742−10756.

(13) Maggini, M.; Scorrano, G.; Prato, M. *J. Am. Chem. Soc.* **1993**, *115*, 9798−9799.

(14) VT ^{1}H NMR experiments have been performed for **6** and **7**, but no appreciable variations of the line width and/or resolution were detected.

(15) ^{13}C NMR spectra have been recorded for **6** and **7**, but no useful information on the carbonyl resonances, which requires long acquisition times or higher sensitivity instruments, could be derived.

(16) The 2D ROESY spectra registered for **6** and **7** (room temperature) did not present any exchange cross peaks, so the precence of (slow) exchange processes between different species can be excluded.

(17) The photophysical characterization of **6** was not carried out, since the photoinduced electron-transfer process from the singlet excited state of the free base porphyrin to the {Re(CO)$_3$(bpy)} is thermodynamically forbidden.[6c]

(18) Fajer, J.; Borg, D. C.; Forman, A.; Dolphin, D.; Felton, R. H. *J. Am. Chem. Soc.* **1970**, *3*, 3451−3459.

(19) DCM as solvent for the laser photolysis experiments exciting at 420 nm was not used since photodegradation was observed under our experimental conditions.

(20) Ghirotti, M.; Chiorboli, C.; You, C. C.; Würthner, F.; Scandola, F. *J. Phys. Chem. A* **2008**, *112*, 3376−3385.

(21) The singlet (E^{0-0} = 1.76 eV) and the triplet (E^{0-0} = 1.50 eV) first excited states of C_{60} are not involved in the deactivation of the singlet excited state ^{*1}ZnP−Re−C_{60}, since neither the transient absorption of the singlet or triplet first excited states of C_{60} nor emissions originating form excited states of C_{60} were observed.

(22) Arrigo, A.; Santoro, A.; Indelli, M. T.; Natali, M.; Scandola, F.; Campagna, S. *Phys. Chem. Chem. Phys.* **2014**, *16*, 818−826.